JOURNAL OF SOLID STATE CHEMISTRY 104, 21–32 (1993)

The Structures of Tb_7O_{12} and $Tb_{11}O_{20}$

J. ZHANG, R. B. VON DREELE,* AND L. EYRING

*Department of Chemistry and Center for Solid State Science, Arizona State University, Tempe, Arizona 85287-1604; and *Manuel Lujan, Jr., Neutron Scattering Center, LANSCE, MS H805, Los Alamos National Laboratory, Los Alamos, New Mexico 87545*

Received October 29, 1992; accepted November 9, 1992.

The structures of Tb_7O_{12} and $Tb_{11}O_{20}$ have been determined by Rietveld analysis of high-resolution neutron diffraction data. Tb_7O_{12} is rhombohedral of space group $R\bar{3}$ with $a = 6.5082(3)$, $\alpha = 99.3420(1)$, $V = 263.32(3)$, and $Z = 1$. This structure is isomorphous with Pr_7O_{12}. $Tb_{11}O_{20}$ is triclinic of space group $P\bar{1}$ with $a = 6.50992(4)$, $b = 9.8298(6)$, $c = 6.4878(4)$, $\alpha = 90.019(2)$, $\beta = 99.966(1)$, $\gamma = 95.881(1)$, $V = 406.68(7)$, and $Z = 1$. Its structure is different than previously proposed. The vacant oxygen coordination sites are not paired across metal atoms. Establishment of these structures will contribute to unraveling the structural principle underlying oxygen-deficient fluorite-related structures.

Personal Tributes to J. S. Anderson

During our (L. E.) first efforts, in the late 1940s and early 1950s, to understand the incomprehensible behavior of the higher rare earth oxides, which seemed not to follow the basic principles of general chemistry at all, we came upon a review in the *Annual Reports of the Chemical Society* by J. S. Anderson titled "Nonstoichiometric Compounds" (*1*). This review introduced us to an aspect of solid state chemistry of which we had been unaware. The work of R. E. Ferguson and E. Daniel Guth on these mystifying Pr and Tb oxides was published (*2, 3*) with confidence having been reassured by Anderson's review.

Had we been aware of the work on the "homologous series" of oxides already being published by A. Magnéli (*4*) or the work of A. D. Wadsley who was describing these series structures in terms of "crystallographic shear" (*5*) we should have been even more confident. Nevertheless, when an opportunity came in 1958 and 1959 to go abroad, arrangements were made to visit Anderson and Wadsley in Melbourne and Magnéli in Stockholm.

L. E. and his family arrived in Melbourne in the Australian spring of 1959 to spend a year with J. S. to find that he had just taken the position of Director of The Chemical Laboratory in England. J. S. had, however, arranged that while we were in Australia our social and cultural affairs would be guided by his generous wife Joan who was yet to join him in England. Our scientific odyssey was to be in the company of some of his young faculty colleagues and graduate students. David Wadsley offered further social and scientific riches. To top it off, two of Anderson's research colleagues (Bruce Hyde and Jim Sawyer) followed me back to the United States to continue my education into modern aspects of solid state chemistry as it pertained to the rare earth oxides. The two years abroad, in the company of those who were writing the book on the behavior of complex solid state inorganic systems, set the direction for my scientific life.

J. S. Anderson was appropriately ac-

0022-4596/93 $5.00

corded the role of guru to the solid state chemistry community on matters concerning nonstoichiometry and ordered intermediate compounds over the whole range of their properties especially their thermodynamic and structural relationships. His reviews and keynote lectures (e.g., *1*, *6–8*) reflect his influence on the field up until near his retirement. His research included thermodynamic studies, properties exploration, and in his later years the revelation of subtle structural features observed by high-resolution electron microscopy.

It is particularly fitting that this report on the Rietveld refinement of the structures of two anion-deficient terbium oxides appears in this volume dedicated to the memory of J. S. Anderson. It was 20 years ago in his laboratory at Oxford that one of us (R. B. V. D.) and A. K. Cheetham first began the use of what is now known as the Rietveld method by applying the technique to the complex structures formed by niobium oxide (*9–12*). These structure refinements were among the first to be reported using this technique and represented a quantum leap in the capability of crystal structure refinements from powder data.

Introduction

In the higher rare earth oxides we see exhibited the special features alluded to above, e.g., wide-range nonstoichiometry and ordered phases that might be termed homologous series. Forty years of research notwithstanding, the true nature of nonstoichiometry and the structural principles that apply to the ordered intermediate phases in these rare earth oxide systems ultimately remain a mystery. The structures are fluorite-related and oxygen-deficient. The main compositional series has the generic formula R_nO_{2n-2} with many examples in the cerium, praseodymium, and terbium oxides. Our attention will be drawn in this paper to the recently determined structures of two members of this series among the Tb oxides.

The series was established by oxygen pressure–temperature–composition studies usually accompanied by X-ray powder diffraction observations (*3*, *13–15*). Later the unit cells were determined by electron microscopy (*16*) and further information on the structures was obtained by high-resolution electron microscopy HREM (*17*). The most advanced information on the structures of Tb_7O_{12} and $Tb_{11}O_{20}$ up to the present came from the HREM image matching that, although convincing at the time, had to be understood as less than definitive. It remains desirable to determine, with certainty, the structures of as many members of the intermediate phases in the Ce, Pr, and Tb oxide series as needed to establish the structural principle relating them. This goal can only be reached by the proper interpretation of high-resolution neutron diffraction data.

Experimental Section

The Preparation of Tb_7O_{12}

The terbium oxide used in this structure determination was purchased from Research Chemicals, Inc., as 5N pure and was processed as follows. The original material, nominally Tb_4O_7, was loaded into a quartz reaction vessel and attached to the preparation system by a standard taper joint. The sample was heated at 800°C while the pressure was reduced cautiously to 1.5×10^{-4} Torr. The temperature was increased to 1009°C for 2 hr, to be certain of complete water and carbon dioxide removal, then decreased to 686°C. The specimen was white, characteristic of the sesquioxide. The pressure was increased to 12.9 Torr and these conditions of temperature and oxygen pressure held for 125 hr before the sample tube was sealed and the specimen cooled. The residual oxygen in the sealed tube was insufficient to change the composition significantly during cooling.

The Preparation of $Tb_{11}O_{20}$

A quantity of the same material used for the Tb_7O_{12} preparation was cautiously heated at 1000°C in a dynamic vacuum to

reduce the oxide to the sesquioxide and to remove the adsorbed carbon dioxide and water. This reduction was carried on for 2 days, at which time the ambience was changed to 380 Torr oxygen pressure and 250°C, and held for 16 days. The final composition was $Tb_{11}O_{20}$, as confirmed by parallel thermogravimetric and tensimetric runs and verified by X-ray powder diffraction analysis. All subsequent operations required to fill and seal the vanadium can for insertion into the neutron diffractometer were performed as before in an inert-gas-filled glove box to prevent contamination.

Powder Neutron Diffraction and Rietveld Analysis

The neutron diffraction data for the above samples were collected on the high-resolution instrument (NPD) at the Manuel Lujan, Jr., Neutron Scattering Center in the Los Alamos National Laboratories in 1989. Each data set includes four time-of-flight spectra with detectors at 2θ of $\pm 148°$ and $\pm 90°$, respectively. The full profile refinements were performed utilizing the GSAS (*18*) structure analysis package.

As Tb_7O_{12} was known to be isostructural with Pr_7O_{12}, the structure of which has been determined (*19*), the structure refinement of Tb_7O_{12} started by employing Pr_7O_{12} as the model. After the background, profile, and diffractometer coefficients were refined, structural parameters including lattice constants and thermal and positional parameters were also allowed to be varied under the constraints of $R\bar{3}$ symmetry.

At a later stage of the refinement, an attempt was made to refine the isotropic thermal parameters of each individual atom independently. However, the resultant U_{iso}'s of the like atoms remained nearly identical whereas the associated standard deviations were twice as high as the values when they were linked. Therefore, in the final refinements, constraints on the isotropic thermal parameters of the cations as well as of the anions were imposed.

As a test of the validity of the $R\bar{3}$ symmetry, the constraints of the 3-fold axis were lifted and small distortions in the lattice constants were introduced arbitrarily. The refinement of this $P\bar{1}$ model was not successful, as indicated by the strong correlations between structural parameters and instability of the least squares refinement.

Although the refinement of the single phase model achieved convergence with acceptable statistical factors (wR_p 5.80%, R_p 4.11%, χ^2 (reduced) 1.992), a close examination of the I_o–I_c curve indicated residual peaks most often located on the larger d-spacing side near the strong fluorite reflections. This implied the existence of a minor phase which might be fluorite related and more reduced than Tb_7O_{12}. It was observed that these residual peaks could be better accounted for if the C-type sesquioxide rather than the simple fluorite was chosen as the second phase. The refined lattice constant of this cubic cell (a = 10.7295(7) Å $\simeq 2a_F$) is not significantly different from that of C-Tb_2O_3 (a = 10.7281(5) Å) (*14*). Nevertheless, it is possible that this second phase is indeed the nonstoichiometric σ phase Tb_2O_{3+x} (x = 0 to 0.38). Due to its low percentage in the sample and the fact that the structure details of the σ phase remain to be clarified, an unambiguous characterization of this minor phase was impossible. However, the model that incorporated 3.7 at.% of the C-type Tb_2O_3 related phase improved the overall statistics of the refinement significantly (Table I).

Figure 1a shows the match between the calculated spectrum based on the two-phase model (solid line) and the observed data (dots) for the $2\Theta = +148°$ bank. The Bragg positions are marked as bars. The positional and thermal parameters of Tb_7O_{12} are reported in Table II, and the important distances are listed in Table III.

Based on the electron microscopic investigations (*16, 17*) and the assumed structural analogies between Pr_7O_{12} and other rare earth oxide intermediate phases, a model was proposed for $Tb_{11}O_{20}$ which had oxygen vacancy pairs that were separated by $\frac{1}{2}\langle 111\rangle_F$ vectors across Tb atoms. This model was similar to the structure of Pr_9O_{16}

TABLE I

IMPORTANT REFINEMENT PARAMETERS FOR Tb_7O_{12}

Diffractometer type		NPD	
No. data		26,009 (4 banks)	
Min. d-spacing (Å)		0.5	
Model		Tb_7O_{12} (96.3%)	Tb_2O_3 (3.7%)
Space group		$R\bar{3}$	$Ia\bar{3}$
Lattice constants:			
a (Å)		6.5082(3)	10.7295(7)
α (°)		99.3420(1)	
V (Å^3)		263.32(3)	1235.2(2)
Z		1	16
Variables:			
Structural:	lattice	2	1
	positional	9	4
	thermal	2	2
Others:	absorption	4	
	background	36	
	diffractometer	11	
	profile	8	
	scale	5	
Total		84	
wR_p[a] %		5.21	
R_p[b] %		3.76	
χ^2 (reduced)[c]		1.611	

[a] $wR_p = [w\Sigma(I_o - I_c)^2/\Sigma wI_o^2]^{1/2}$.
[b] $R_p = \Sigma|I_o - I_c|/\Sigma I_o$.
[c] $\chi^2 = \Sigma w(I_o - I_c)^2/(N_{obs} - N_{var})$.

TABLE II

POSITIONAL AND THERMAL PARAMETERS FOR Tb_7O_{12}

Atom	x	y	z	$U_{iso} \times 100$ (Å^2)[a] (linked)
Tb(1)	0	0	0	0.61(1)
Tb(2)	0.30466(9)	0.13852(9)	0.60594(8)	0.61(1)
O(1)	0.9259(1)	0.0605(2)	0.6824(1)	1.21(1)
O(2)	0.5687(1)	0.4163(2)	0.8220(1)	1.21(1)
Vacancy	$\frac{1}{4}$	$\frac{1}{4}$	$\frac{1}{4}$	—

[a] The form of the isotropic displacement parameter is $T = \exp[-8\pi^2 U_{iso} \sin^2\theta/\lambda^2]$.

(*17*, *20*) except that the vacancy pairs are further diluted with TbO_2 groups in between. Refinements based on this model and later on another model with such vacancy pairs oriented in a different direction failed to fit the observed neutron diffraction data to a satisfactory level (wR_p 7%, χ^2 (red.) 4.5 or higher), and unreasonably short distances were observed, as was often experienced for unsuccessful refinements. Reexamination of this system revealed that, limited by the size of the $P\bar{1}$ symmetry of the unit cell, there were five possible vacancy models for $Tb_{11}O_{20}$, of which the two with the vacancy pairs had already been eliminated as mentioned

TABLE III

IMPORTANT INTERATOMIC DISTANCES IN Tb_7O_{12}

Atom 1	Atom 2	Mult.	Distance (Å)	Atom 1	Atom 2	Mult.	Distance (Å)
			Tb coordination environment				
Tb(1)	O(1)	6	2.1589(9)	Tb(2)	O(1)	1	2.580(1)
(CN = 6)				(CN = 7)		1	2.262(1)
						1	2.268(1)
					O(2)	1	2.283(1)
						1	2.362(1)
						1	2.295(1)
						1	2.212(1)
					average		2.323
			O vacancy cluster				
V_O	Tb(1)	1	2.3158(7)	Tb(1)	Tb(2)	3	4.0027(9)
	Tb(2)	3	2.5260(5)	Tb(1)	Tb(2)	3	4.0722(9)
	average		2.4734		average[a]		4.0375
V_O	O(1)	3	2.2996(9)				
	O(2)	3	2.4506(9)				
	average		2.3751				

[a] The average Tb–Tb distance within the V_OTb_4 group.

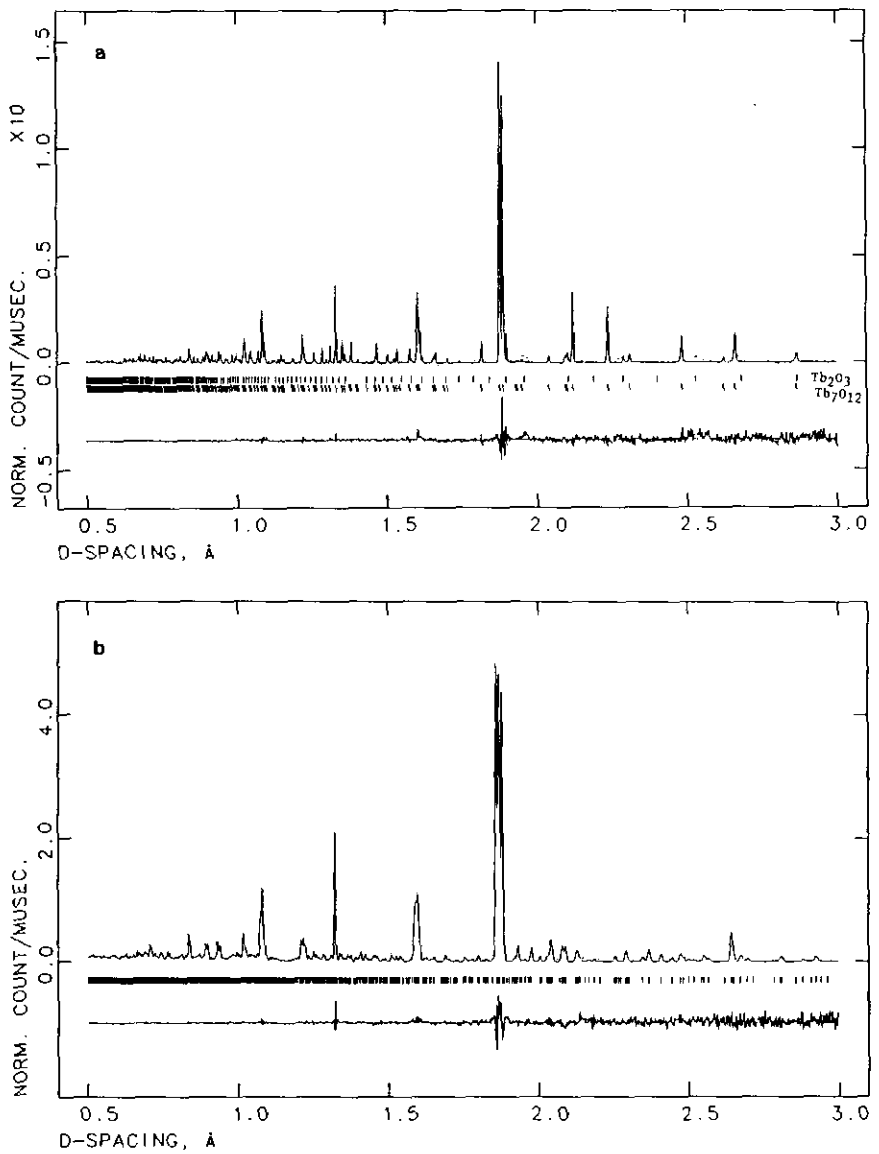

FIG. 1. The observed (dots) and calculated (solid lines) powder neutron diffraction profiles for Tb_7O_{12} (a) and $Tb_{11}O_{20}$ (b). The Bragg positions are marked as bars.

above. Among the three models left, the one with larger separations between the isolated vacant oxygen sites seemed more plausible than the rest which had oxygen vacancies separated by $\frac{1}{2}(111)_F$ vectors but no metal atoms in between. Further refinement of this model was successful (Table IV) and compared with the other four possibilities tested, its agreement with the observed spectra was significantly better. As shown in Fig. 1b, the calculated spectrum (solid line) is in good agreement with the observed data (points), and a few residue peaks under the strong Bragg reflections are presumably due to inadequate modeling of these profiles. No impurity phase was found. Important distances are listed in Table V.

TABLE IV

IMPORTANT REFINEMENT PARAMETERS FOR $Tb_{11}O_{20}$

Diffractometer type		NPD
No. data		25,990 (4 banks)
Min. d-spacing (Å)		0.5
Model		$Tb_{11}O_{20}$ (100%)
Space group		$P\bar{1}$
Lattice constants:		
a, b, c (Å)		6.50992(4), 9.8298(6), 6.4878(4)
α, β, γ (°)		99.019(2), 99.966(1), 95.881(1)
V (Å^3)		406.68(7)
Z		1
Variables:		
Structural:	lattice	6
	positional	45
	thermal	2 (linked)
Others:	absorption	4
	background	36
	diffractometer	11
	profile	8
	scale	4
Total		116
wR_p %[a]		4.26
R_p %[b]		3.12
χ^2 (reduced)[c]		1.236

[a] $wR_p = [w\Sigma(I_o - I_c)^2/\Sigma wI_o^2]^{1/2}$.
[b] $R_p = \Sigma|I_o - I_c|/\Sigma I_o$.
[c] $\chi^2 = \Sigma w(I_o - I_c)^2/(N_{obs} - N_{var})$.

Results and Discussion

Tb_7O_{12}

Successful Rietveld analysis of the neutron diffraction data has proven that Tb_7O_{12} and Pr_7O_{12} are isostructural. The lattice constants of the rhombohedral cell (Table I) are in good agreement with those obtained from X-ray powder diffraction, and the fractional position parameters (Table II) differ only slightly from those of Pr_7O_{12} to accommodate the decrease in the size of the cation.

Similarly to Pr_7O_{12}, the oxygen vacancy pairs along $\langle 111\rangle_F$ direction across a metal atom can be considered as the basic building blocks for Tb_7O_{12} (Fig. 2a). The center of the vacancy pair is fixed at one inversion center and a trigonal, centrosymmetric distortion of the rest of the Tb sublattice is observed. The Tb(2) cations are moved away from the nearest oxygen vacancy (V_O), which bears a formal positive charge, by 0.2 Å, which results in an average Tb–Tb distance of 4.04 Å for the Tb atoms associated with a particular vacancy. The average distance between those Tb cations that belong to different vacancy clusters is decreased to 3.6 Å from the value of 3.76 Å if the ideal fluorite structure is assumed. It is worthwhile to note that the lattice of Tb_7O_{12} may be divided into two sections. As shown in Fig. 2a, although the shortest separation between the nearest oxygen vacancies is $\frac{1}{2}[111]_F$ in both regions A and B, the distribution of the electrostatic repulsion in the cation sublattice is not uniform. In region A, two V_OTb_4 groups share a common Tb atom at the origin, and the expansion of the V_OTb_4 groups is mainly away from each other. On the other hand, the V_OTb_4 groups in region B become closer to each other due to the lattice distortion, resulting in higher electrostatic repulsion in this area. This observation is consistent with the fact that in the more oxidized intermediate rare earth oxides such as Pr_9O_{16} (*20*) and $Pr_{10}O_{18}$ (*20*), the structure fragment A is preserved while the less stable features in region B no longer exist.

From another point of view, the structure

TABLE V

POSITIONAL AND THERMAL PARAMETERS FOR $Tb_{11}O_{20}$

Atom	x	y	z	$U_{iso} \times 100$ (Å^2)[a] (linked)
Tb(1)	0	0	0	0.38(1)
Tb(2)	0.1020(3)	0.3629(2)	0.1786(4)	0.38(1)
Tb(3)	0.5536(4)	0.1704(2)	0.1208(3)	0.38(1)
Tb(4)	0.6380(3)	0.5223(2)	0.2732(3)	0.38(1)
Tb(5)	0.1380(3)	0.7219(2)	0.3594(3)	0.38(1)
Tb(6)	0.7365(3)	0.9206(2)	0.4762(3)	0.38(1)
O(1)	0.3607(4)	0.0459(3)	0.8529(5)	0.78(1)
O(2)	0.8198(4)	0.1991(3)	0.9539(4)	0.78(1)
O(3)	0.4392(4)	0.3728(3)	0.0419(5)	0.78(1)
O(4)	0.9398(5)	0.5654(3)	0.1609(5)	0.78(1)
O(5)	0.0330(4)	0.9286(3)	0.3461(5)	0.78(1)
O(6)	0.2313(5)	0.1508(3)	0.2000(5)	0.78(1)
O(7)	0.7953(5)	0.3312(3)	0.3114(5)	0.78(1)
O(8)	0.3369(4)	0.5504(3)	0.3702(5)	0.78(1)
O(9)	0.8128(5)	0.7076(3)	0.4537(5)	0.78(1)
O(10)	0.4051(5)	0.8715(3)	0.5262(5)	0.78(1)
Vacancy	$\frac{1}{2}$	$\frac{3}{4}$	$\frac{1}{2}$	—

[a] *The form of the isotropic displacement parameter is* $T = \exp[-8\pi^2 U_{iso} \sin^2\theta/\lambda^2]$.

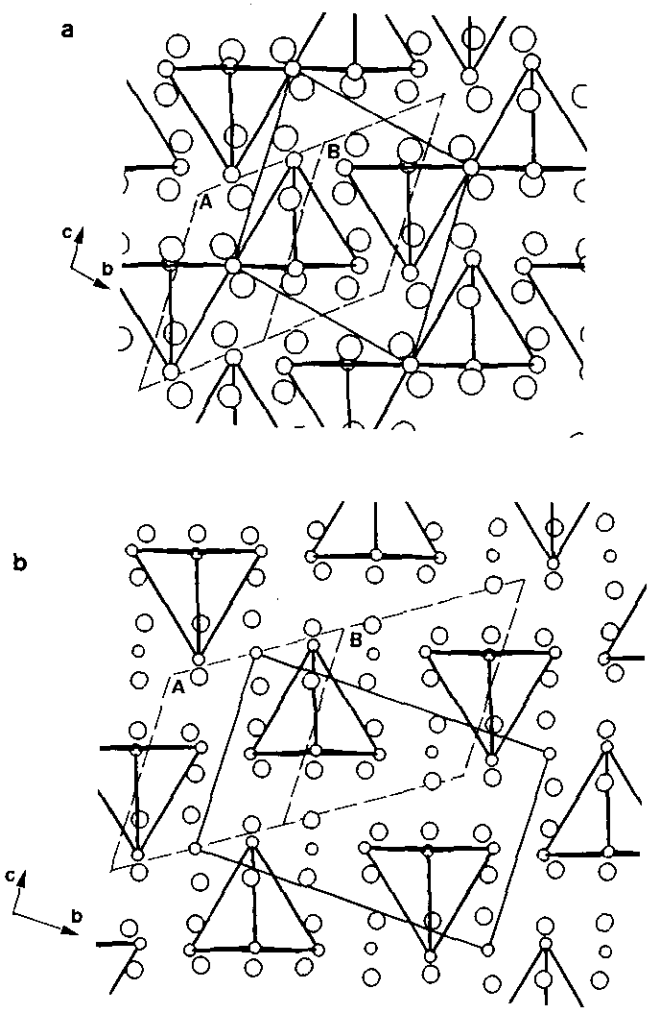

FIG. 2. The refined structural models of Tb_7O_{12} (a) and $Tb_{11}O_{20}$ (b) projected along their a axes (generated via ORTEP, 99% thermal ellipsoids).

of Tb_7O_{12} may be described by employing the concept of the coordination defect proposed by Hoskins and Martin (*21–23*). This model focuses on the defect and relaxation of the anion lattice and suggests that the strong polarization around a vacant oxygen site makes the six nearest oxygen neighbors coordinate to the defect center. The complex involving seven oxygen positions then exists as one structural entity. In Tb_7O_{12}, the six oxygen atoms move toward the vacant site, giving an average V_O–O distance which is about 0.3 Å below the average 0–0 distance of 2.66 Å (Table III). With a formal composition of $Tb_{7/2}O_6$, these coordination defects are arranged in Tb_7O_{12} in a closest packed manner. There are no other structural elements than $Tb_{7/2}O_6$ as is the case for higher intermediate oxides, and sharing oxygen atoms between the coordination defects was forbidden and therefore not observed. Considering such oxygen vacancy clusters as the basic building blocks, one may realize that slabs of vacancies in the $(153)_F$ plane could be obtained via close packing of individual vacancies in the a and

c directions. In Tb_7O_{12}, these slabs are stacked to fill the space. However, as discussed above, the electrostatic interaction is not evenly distributed between pairs of slabs. Therefore, it is reasonable to expect that in the higher oxides, the separation of the slabs would first occur in region B where repulsion is greater, and then in region A upon further oxidation.

As in Pr_7O_{12}, there are two types of cations in the structure. The six-coordinated Tb(1) carries a +4 formal charge suggested by the Tb–O distance (Table III). The average Tb(2)–O distance is, on the other hand, between the values of the sum of the crystal radii for a +3 and +4 Tb (CN = 7), and for each of the six symmetry related Tb(2) in one unit cell, a formal state of +3.33 is required by the composition. It might be possible that the six seven-coordinated Tb cations were actually two +4 and four +3 ions related by a symmetry operation that is lower than 3 and the mixed valence state was imposed by the pseudo-3-fold axis. However, the structural refinement did not provide any evidence supporting this hypothesis. Since the refinement was based on powder rather than single crystal diffraction data, problems of twinning should be irrelevant. Therefore, the observed $R3$ symmetry may be interpreted either as an indication of the true mixed valence state for Tb(2) or as the result of fast electron hopping among the +4 and +3 Tb cations. As the neutron data were collected over a period much longer than the time scale of the electron transfer, the individual valence states could not be resolved via this method, yielding a statistical structural model with the mixed valence state. It is worth pointing out that dynamic disorder is possible in Tb_7O_{12} since the U_{iso}'s in this structure are roughly double the corresponding values in $Tb_{11}O_{20}$. X-ray absorption spectroscopic studies (*24*) of the higher oxides of terbium have been interpreted as showing only Tb^{3+} and Tb^{4+} species, that is, no cations of intermediate valence. Presumably, this reflects the instantaneous states, whereas the neutron diffraction results reflect the average states.

$Tb_{11}O_{20}$

Contrary to the assumption that the intermediate rare-earth oxides in the Pr–O and Tb–O systems share the oxygen vacancy pair as the common structural element, the neutron diffraction study and the subsequent Rietveld analysis have shown that $Tb_{11}O_{20}$ consists of individual vacant oxygen sites that are distributed in a more uniform manner (Fig. 2b). This discovery is consistent with the structure study on β_1-$Pr_{12}O_{22}$ (*20*) and suggests that the validity of the vacancy pair model may be confined only to the more reduced oxides in these binary systems. In addition, the fact that $Tb_{11}O_{20}$ and $Pr_{12}O_{22}$ belong to different subgroups divided on the basis of symmetry or whether the oxide is an even or odd member in the R_nO_{2n-2} series suggests that, despite the differences in the unit cell dimensions or symmetries, the structures of the intermediate oxides are governed to a large extent by the electrostatic repulsions between the vacancies or the defect clusters.

Figure 2b is the projection of $Tb_{11}O_{20}$ along the a axis. Similar to what is observed for $Pr_{12}O_{22}$, the vacant oxygen sites are distributed in a way such that separations between the defects are maximized and therefore the repulsive interactions are reduced. Furthermore, the breaking up of a vacancy pair allows all four of the surrounding Tb cations to relax in a more isotropic way (Tb–V_O ranges 2.45–2.56 Å). In addition, an increase in the number of structural entities by the dissociation of a pair of vacant sites may also contribute to the increase in the entropy which would further stabilize the structure.

The distortion of the oxygen sublattice again supports the model utilizing coordination defects, suggested by Hoskins and Martin (*21–23*). The six nearest oxygens in the vicinity of a vacant site move toward the center of the defect with an average O–V_O distance of 2.3 Å, whereas the distances

between the oxygen atoms in this structure are above 2.6 Å with only one exception (O(5)–O(5), 2.562 Å). These defect complexes are distributed apart from each other in order to minimize repulsions and to relieve lattice tension, and the shortest separation between any oxygen vacancies is $\frac{1}{2}[012]_F$.

The relaxation of the Tb sublattice, on the other hand, is also important to the structural stability. Similarly to the other known structures of the intermediate phases, the vacant Tb_4 tetrahedron expands and the regions between such Tb_4 groups experience substantial compression indicated by the differences between the average intragroup distance (4.1 Å) and the intergroup distance (3.6 Å). There are also Tb atoms that are not directly associated with a vacancy, as required by the composition. These independent Tb atoms exist between the vacant Tb_4 groups and may be considered as buffers to reduce the tension among the Tb_4 groups. With the coordination number of 8 and the average distance to the Tb neighbors of 3.71 Å, the coordinates of these Tb atoms are essentially identical to those in the ideal fluorite. Restricted by the cell dimensions and symmetry, the positions of the Tb_4 groups as well as the eight-coordinated Tb cations lead to an uneven distribution of the strains in the Tb sublattice. Although the shortest vacancy–vacancy separations in this structure are all of the $\frac{1}{2}\langle 012\rangle_F$ type, two nonequivalent structure configurations may be derived which differ from each other in the relative orientation of the Tb_4 groups around oxygen vacancies and the cation lattice. Judged on the basis of the Tb–Tb distances and the fact that there are more isolated Tb^{3+} cations between Tb_4 groups, the stress in region B should be less significant than that in region A (Fig. 2b). In fact, the Tb(6) in region A has six intergroup short Tb–Tb distances with the average of 3.59 Å while other Tb cations in the Tb_4 group each have only five nearest neighbors at an average distance larger than 3.6 Å. Apparently, the tension in the cation sublattice has affected the anion sublattice, too, for the shortest O–O distance in this structure, O(5)–O(5) of 2.562 Å, is also observed in region A. As may be expected, stress of such a nature would increase with the size of the cation, and this might be the reason that the isostructural praseodymium phase has not been observed. $Pr_{11}O_{20}$ with a similar $P\bar{1}$ cell may have too much tension in region A to be stable, and therefore adopts an unknown structure with a larger cell. It also explains the fact that, although the vacancies are separated by the same $\frac{1}{2}[012]_F$ vectors in both regions, the type of arrangement in region B has been observed in the structure of β_1-$Pr_{12}O_{22}$ whereas that in region A has not.

The structure of $Tb_{11}O_{20}$ may also be described as the stacking of the (153) vacancy slabs as observed in Tb_7O_{12} except that they are no longer closely packed due to oxidation. In both regions A and B, pairs of vacancy slabs are separated by layers with the composition TbO_2 (Fig. 2b), except that the amount of TbO_2 in region B is twice that in region A. This representation is consistent with the analysis based on the Tb–Tb distances and suggests that configuration B is relatively more stable than configuration A.

The charge distribution in the cation lattice of $Tb_{11}O_{20}$ is another interesting aspect. By comparing the average Tb–O distances (Table VI) with the corresponding sum of crystal radii (*25*), it is suggested that the two eight-coordinated Tb cations carry formal charges of +3. Among the four Tb atoms in each empty Tb_4 group, Tb(5) and Tb(6) in the region with high lattice tension may be considered as Tb^{4+}, while Tb(3) and Tb(4) in region B have an average charge of 3.75 to achieve electrical neutrality. As expected, this assignment suggests that the charge distribution depends strongly on structural features such as coordination numbers and lattice distortions. Without any imposed symmetry, the less pronounced charge differences within the Tb_4 group could suggest the existence of mixed

TABLE VI

IMPORTANT INTERATOMIC DISTANCES IN $Tb_{11}O_{20}$

Atom 1	Atom 2	Mult.	Distance (Å)	Atom 1	Atom 2	Mult.	Distance (Å)
			Tb coordination environment				
Tb(1)	O(1)	2	2.680(3)	Tb(2)	O(2)	1	2.560(4)
CN = 8	O(2)	2	2.375(3)	CN = 8	O(3)	1	2.498(4)
	O(5)	2	2.332(3)		O(4)	1	2.339(4)
	O(6)	2	2.238(4)		O(4)	1	2.291(4)
	average		2.406		O(6)	1	2.321(4)
					O(7)	1	2.300(4)
					O(8)	1	2.457(4)
					O(9)	1	2.469(4)
					average		2.404
Tb(3)	O(1)	1	2.251(4)	Tb(4)	O(3)	1	2.289(4)
CN = 7	O(1)	1	2.240(4)	CN = 7	O(3)	1	2.240(4)
	O(2)	1	2.191(4)		O(4)	1	2.212(4)
	O(3)	1	2.223(4)		O(7)	1	2.223(4)
	O(6)	1	2.234(4)		O(8)	1	2.201(4)
	O(7)	1	2.306(5)		O(8)	1	2.404(4)
	O(10)	1	2.300(4)		O(9)	1	2.256(4)
	average		2.249		average		2.261
Tb(5)	O(2)	1	2.226(4)	Tb(6)	O(1)	1	2.153(4)
CN = 7	O(4)	1	2.169(4)	CN = 7	O(5)	1	2.172(4)
	O(5)	1	2.206(3)		O(5)	1	2.229(4)
	O(7)	1	2.178(4)		O(6)	1	2.197(4)
	O(8)	1	2.221(4)		O(9)	1	2.210(4)
	O(9)	1	2.293(3)		O(10)	1	2.240(4)
	O(10)	1	2.275(4)		O(10)	1	2.324(4)
	average		2.224		average		2.218
			O vacancy cluster				
V_O	Tb(3)	1	2.506(2)	Tb(3)	Tb(4)	1	4.107(4)
	Tb(4)	1	2.489(2)		Tb(5)	1	4.071(3)
	Tb(5)	1	2.564(2)		Tb(6)	1	4.059(3)
	Tb(6)	1	2.453(3)	Tb(4)	Tb(5)	1	4.083(3)
	average		2.503		Tb(6)	1	4.080(3)
				Tb(5)	Tb(6)	1	4.120(3)
V_O	O(1)	1	2.264(3)		average[a]		4.087
	O(2)	1	2.364(3)				
	O(3)	1	2.356(3)				
	O(8)	1	2.332(3)				
	O(9)	1	2.303(3)				
	O(10)	1	2.355(3)				
	average		2.329				

[a] The average distance within the $V_O Tb_4$ group.

valence states or fast electron transfer between cations, similar to that discussed for Tb_7O_{12}. It also may imply that the even charge distribution in Tb_7O_{12} is the cause of the observed $\bar{3}$ symmetry, not the result.

The structural characterization of Tb_7O_{12} and $Tb_{11}O_{20}$ suggests that many of the assumptions of the past are untrue. In a sense these rare earth oxide series are not really homologous. They do not have a structural

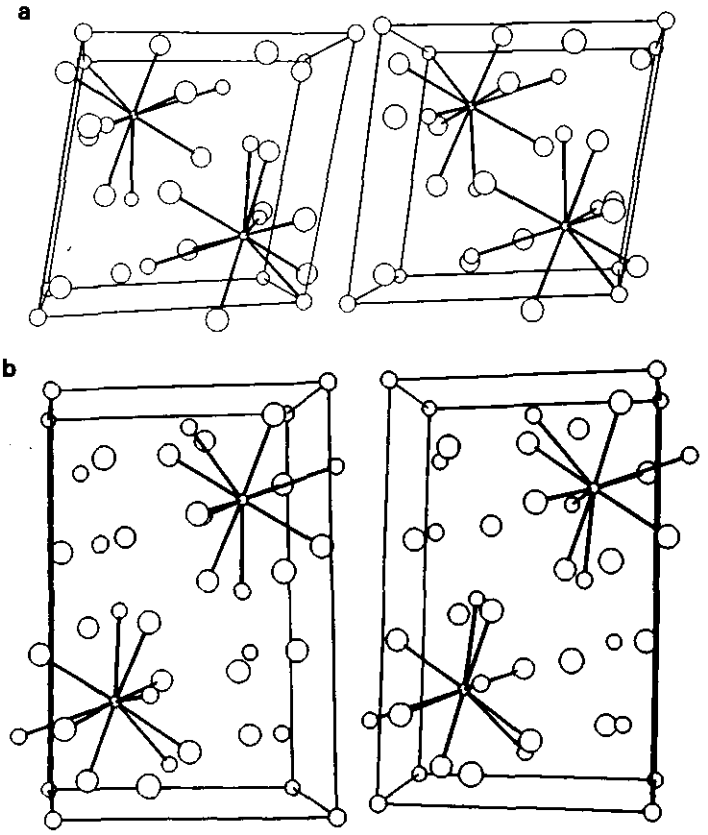

FIG. 3. The stereographs for Tb_7O_{12} (a) and $Tb_{11}O_{20}$ (b). The four Tb cations and six oxygen anions in the vicinity of a vacant oxygen site are corrected to the center of the defect (small circles).

feature, such as a *CS* plane, that is repeated at various intervals to generate the members of the series. Although this characteristic could be said to apply to the members with $n = 7$ and 9 in the PrO_x series, it is not at all general. In the case of TbO_x and a–c planar defect slab is different as between $n = 7$ and 11. The most general identifiable structural defect in these anion-deficient fluorite-related series is a cluster consisting of a vacant oxygen site, its four nearest cation neighbors, and its six nearest oxygen neighbors (Fig. 3a,b).

The occurrence of the odd- and even-type structures that characterize these systems do not correlate with whether or not the vacant oxygens are paired across a metal atom or exist individually throughout the structure. All systems begin with the odd R_7O_{12} primitive structures and apparently none of them switch back to the odd forms after they have gone even. The only demonstrated isostructure so far established is that of R_7O_{12} for all three series. Other possibilities are $R_{11}O_{20}$ in the Tb and Ce systems, $R_{12}O_{22}(3)$ between Tb and Pr oxides, and $R_{31}O_{56}$ between Tb and Ce and possibly Pr.

The possibility that $Tb_{11}O_{20}$ and $Ce_{11}O_{20}$, which have the same unit cells, might be isostructural yet $Pr_{11}O_{20}$ is not, suggests that the atomic interactions depend on more than atomic size.

Acknowledgments

We acknowledge the National Science Foundation for support for Research Grants DMR-8820017 and

DMR-9114799, Grant DMR-9115680 for the Center for HREM at Arizona State University, and support from U.S. Government Contract W-7405-ENG-36 for the Los Alamos National Laboratory and the Manuel Lujan, Jr., Neutron Scattering Center. We thank J. Tong for assistance in specimen preparation.

References

1. J. S. ANDERSON, *Annu. Rep. Prog. Chem.* **43,** 104 (1946).
2. R. E. FERGUSON, E. DANIEL GUTH, AND L. EYRING, *J. Am. Chem. Soc.* **76,** 3890 (1954).
3. E. DANIEL GUTH AND L. EYRING, *J. Am. Chem. Soc.* **76,** 5242 (1954).
4. A. MAGNÉLI, *Acta Crystallogr.* **6,** 495 (1953).
5. A. D. WADSLEY, *J. Proc. R. Soc. N. S. W.* **92,** 25 (1958).
6. J. S. ANDERSON, *Am. Chem. Soc. Adv. Chem.*, No. 39, 1 (1963).
7. J. S. ANDERSON, *Proc. Chem. Soc.*, 166 (1964).
8. J. S. ANDERSON, *Proc. Indian Acad. Sci. Chem. Sci.* **93,** 861 (1984).
9. A. K. CHEETHAM AND R. B. VON DREELE, *Nature Phys. Sci.* **244,** 139 (1973).
10. J. S. ANDERSON, J. M. BROWNE, A. K. CHEETHAM, R. B. VON DREELE, J. L. HUTCHISON, F. J. LINCOLN, D. J. M. BEVAN, AND J. STRÄHLE, *Nature* **243,** 81 (1973).
11. J. S. ANDERSON, D. J. M. BEVAN, A. K. CHEETHAM, R. B. VON DREELE, J. L. HUTCHISON AND J. STRÄHLE, *Proc. London Ser. Soc. A* **346,** 139 (1975).
12. R. B. VON DREELE AND A. K. CHEETHAM, *Proc. R. Soc. London Ser. A* **38,** 311 (1974).
13. E. D. GUTH, J. R. HOLDEN, N. C. BAENZIGER, AND L. EYRING, *J. Am. Chem. Soc.* **76,** 5239 (1954).
14. N. C. BAENZIGER, H. A. EICK, H. S. SCHULDT, AND L. EYRING, *J. Am. Chem. Soc.* **83,** 2219 (1961).
15. B. G. HYDE AND L. EYRING, *in* "Rare Earth Research III" (L. Eyring, Ed.), p. 623, Gordon & Breach, New York (1964).
16. P. KUNZMANN AND L. EYRING, *J. Solid State Chem.* **14,** 229 (1975).
17. R. T. TUENGE AND L. EYRING, *J. Solid State Chem.* **41,** 75 (1982).
18. A. C. LARSON AND R. B. VON DREELE, "GSAS—General Structure Analysis System," Los Alamos National Laboratory Report LA-UR 86-748 (1986).
19. R. B. VON DREELE, L. EYRING, A. L. BOWMAN, AND J. L. YARNELL, *Acta Crystallogr. Sect. B* **31,** 971 (1975).
20. J. ZHANG, R. B. VON DREELE, AND L. EYRING, unpublished results.
21. R. L. MARTIN, *J. Chem. Soc. Dalton Trans.*, 135 (1974).
22. B. F. HOSKINS AND R. L. MARTIN, *J. Chem. Soc. Dalton Trans.*, 576 (1975).
23. B. F. HOSKINS AND R. L. MARTIN, *J. Chem. Soc. Dalton Trans.*, 676 (1976).
24. R. C. KARNATAK, J. M. ESTEVA, H. DEXPERT, M. GASGNIER, P. E. CARO, AND L. ALBERT, *Phys. Rev. B* **36,** 1745 (1987).
25. R. D. SHANNON, *Acta Crystallogr. Sect. A* **32,** 751 (1976).